

Current efficiency and selectivity reduction caused by co-ion leakage in electromembrane processes

Junghyo Yoon^a, Matthew T. Flavin^{a,b}, Jongyoon Han^{a,*}

^a Department of Electrical Engineering and Computer Science, Massachusetts Institute of Technology, 77 Massachusetts Avenue, Cambridge, MA 02139, USA

^b The Charles Stark Draper Laboratory, 555 Technology Square, Cambridge, MA 02139, USA

ARTICLE INFO

Keywords:

Electromembrane
Current efficiency
Ion concentration polarization
Hydrodynamic convection
Co-ion leakage

ABSTRACT

In electromembrane processes such as electrodialysis (ED) and ion concentration polarization (ICP), the diffusion layers on both diluate and concentrate sides influence permselectivity of the ion-exchange membrane and current utilization. The diffusion layer in the diluate stream, due to lower salinity and higher resistivity, has been regarded as the primary source of energy loss. In contrast, very few studies have focused on the diffusion layer in the concentrate stream. In this paper, we evaluate the influence of hydrodynamic convective flow on the development of diffusion layers on both concentrate and diluate sides, specifically in the ICP desalination process. Interestingly, the higher convective flow in the concentrate side was shown to drastically improve the current utilization drop in high operating current, which has been a recurring challenge in electromembrane processes. We attribute this to the prevention of co-ion leakage into the membrane, confirmed by both experimentation and numerical modeling. This new insight has a clear design implication for optimizing electromembrane processes for higher energy efficiency.

1. Introduction

Electrodialysis (ED, Fig. 1a) is a mature desalination technology, which has diluate and concentrate compartments separated by alternating two ion-exchange membranes, anion-exchange membrane (AEM) and cation-exchange membrane (CEM), allowing selective ion transport (Strathmann, 2010). It has been widely applied in food processing, seawater desalination, and brine effluent treatment (Fidaleo and Morosi, 2006; Korngold et al., 2009; Sadrzadeh and Mohammadi, 2008). The selective ion transport develops diffusion layers (also known as ion concentration polarization) next to AEM and CEM, which lead to ion removal or concentration downstream. The diffusivity of ionic species is one of the significant factors in developing the diffusion layer in the diluate compartment. It has been experimentally and theoretically proven that the diffusion layer next to CEM ($\delta_{D,CEM}$) is thicker than the diffusion layer next to AEM ($\delta_{D,AEM}$) with a sodium chloride solution ($\delta_{D,CEM} > \delta_{D,AEM}$, Fig. 1a), due to the higher diffusivity of chloride ($t^{Cl^-} = 0.606$), compared to that of sodium ($t^{Na^+} = 0.393$), the majority ions in seawater (Kwak et al., 2013; Shaposhnik et al., 1997, 1995). Based on this scientific insight, we discovered and reported the novel Ion Concentration Polarization (ICP) process, which utilizes only CEMs to

achieve an improved current utilization (CU), also known as current efficiency, than ED ($CU_{ICP} > CU_{ED}$)(Fig. 1b) (Al-anzi et al., 2020; Choi et al., 2019; Kim et al., 2017; Kwak et al., 2016; Yoon et al., 2019). Ideally, CU in ED is $CU = 1$ at zero current limit, but CU in ICP processes is improved as 1.2 at zero current limit with sodium chloride solution, due to its diffusivity mismatch (e.g., chloride diffusivity is higher than that of sodium) (Kwak et al., 2016).

The selective ion transport through ion-exchange membranes creates diffusion layers on both depleted (depletion layer) and concentrated (concentration layer) sides of the membrane, which is the fundamental phenomenon that enables both ED and ICP processes. It is well understood that a thicker ion depletion region (as a result of the higher operating current) is often associated with increased cell resistivity, resulting in additional voltage drop/energy loss. To mitigate this, spacers are added to diluate channel for enhanced mixing, or the flow speed is increased to minimize the boundary layer thickness (Balster et al., 2010, 2006). Another significant loss mechanism in electromembrane processes is the precipitous drop in CU, in proportion to the applied current, which is ubiquitously observed in experimental works on ED and ICP processes (Doornbusch et al., 2020; Kim et al., 2017, 2016; Tanaka, 2000; Yoon et al., 2019). However, understanding of the

* Corresponding author.

E-mail address: jyhan@mit.edu (J. Han).

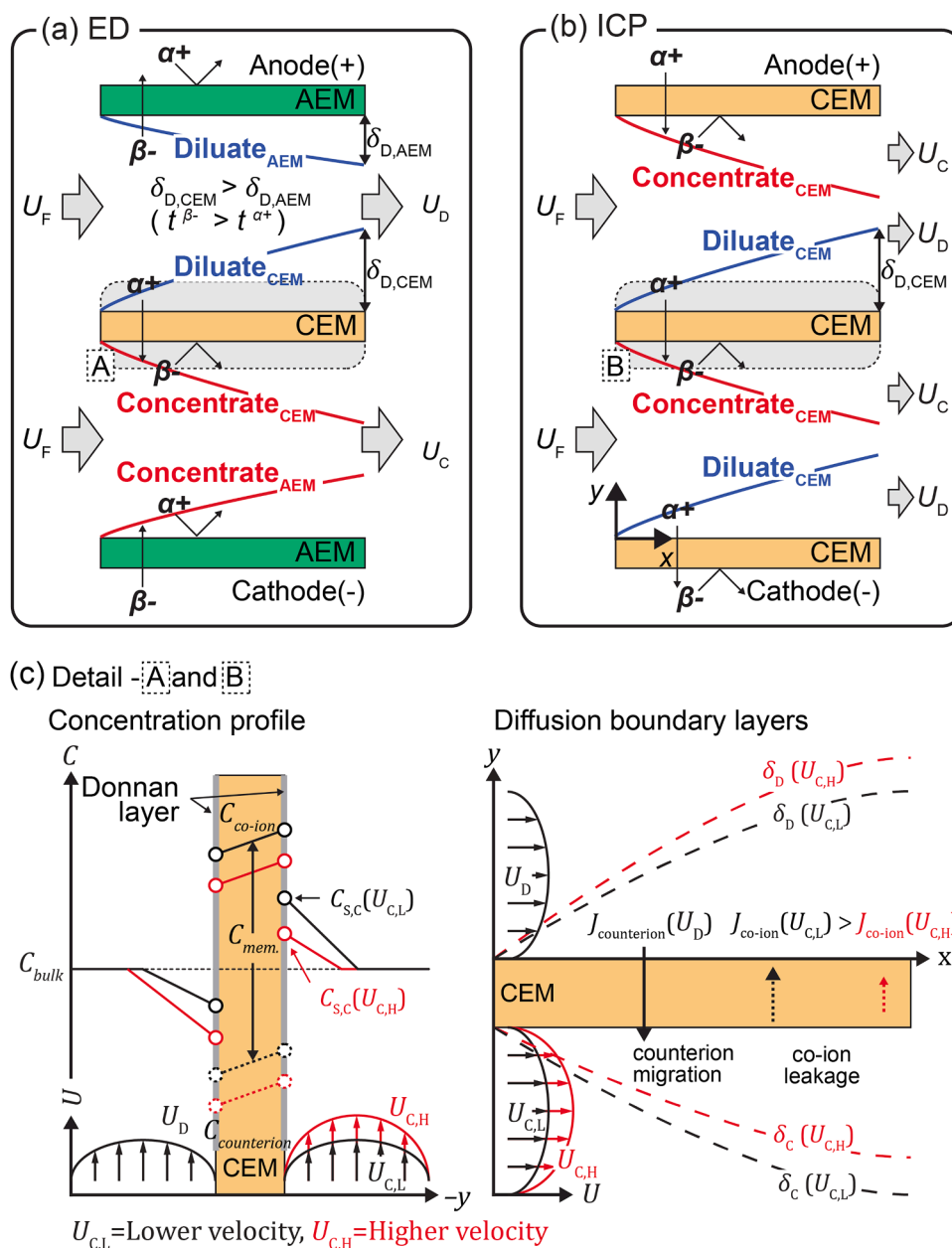


Fig. 1. Schematic illustration of ion transport and flow path in (a) electrodesialysis (ED) and (b) Ion Concentration Polarization (ICP) process. (c) Details of A in (a) and B in (b), the development of diffusion layers on both diluate (δ_D) and concentrate (δ_C) sides and the change in concentration profiles by various flow velocities in concentrate stream (U_C). $J_{counterion}$ and J_{co-ion} indicates transport of counterion and co-ion, respectively.

mechanism behind this has been less than desired. Various second-order phenomena have been suggested as the main reason for the drop in CU, including (1) new current carrier generation (e.g., water splitting) (Nikonenko et al., 2010; Rubinstein and Shtilman, 1979) and (2) membrane discharging by thicker depletion layer (Andersen et al., 2012; Frilette, 1957), and (3) large trans-membrane concentration difference leading to strong back-diffusion and osmosis (Chehayeb et al., 2017). However, as our analysis indicates, none of these effects are large enough to explain dramatic reduction in CU.

CU value of the membrane is directly related to the ion permselectivity of the membrane, and the selectivity of commonly used ED membranes are generally high (>97%) at equilibrium condition (zero current limit). Therefore, a deterioration in CU must be related to a loss in selectivity, specifically, leakage of co-ions under a high current operation. Even at equilibrium, increased salinity around cation exchange membranes (CEMs), compared with the inherent fixed anion

concentration in the membrane, will lead to more anions penetrating into the membrane, governed by Donnan partitioning (Geise et al., 2012). Abu-Rjal et al. developed a simple analytical model demonstrating that a thicker boundary layer on the concentrate side reduces membrane permselectivity (abu-Rjal et al., 2014). However, there has not been any experimental study on this topic, not to mention any strategy to mitigate this selectivity loss for more optimal electro-membrane operation.

It has been experimentally demonstrated, by many researchers, that higher hydrodynamic flow speed (U_H) in ED and ICP improves the overall energy efficiency as well as the current efficiency (La Cerva et al., 2018; Nakayama et al., 2017; Yoon et al., 2019). Previous studies in ED have mainly focused on the reduction of depletion layer thickness by increasing the flow speed (U_D) in the diluate channel (since $\delta \sim \sqrt{Dx/U}$), or by employing mesh spacers (as a turbulence promoter) or corrugated membrane (Balster et al., 2010; Tadimeti et al., 2016).

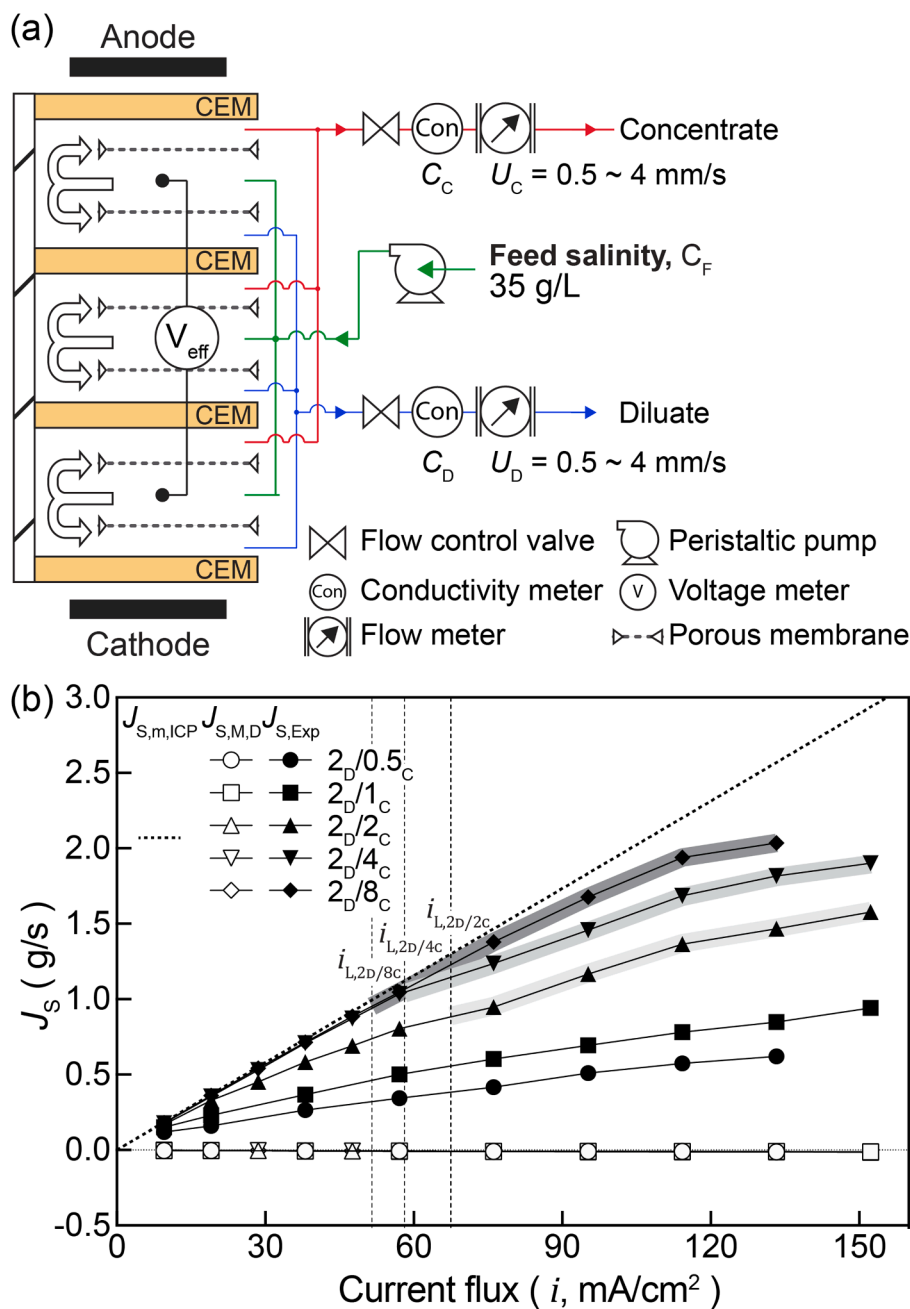


Fig. 2. (a) Schematic of measurement system for analytic experiment of ICP system. (b) The salt flux by electro- and diffusive migrations ($J_{S,m,ICP}$) and trans-membrane diffusion ($J_{S,m,D}$), and the experimental result ($J_{S,Exp}$). A_D/B_C indicates the experiment condition with A mm/s of U_D and B mm/s of U_C . Areas shaded in gray indicate the operating conditions beyond the limiting current regime (The intensity of the grayscale was adjusted to distinguish the conditions.).

Numerical analyses for reverse electrodialysis show that a higher hydrodynamic flow speed leads to a decrease in the system resistance (Moya, 2016) and an improved counter ion transport (Tedesco et al., 2016). Also, the multi-stage ED has been actively investigated to diminish thicker diffusion layers that may result from the single-stage ED (Doornbusch et al., 2019; Jiang et al., 2014; Yan et al., 2019). However, the control of hydrodynamic flow in the concentrate stream (U_C) didn't receive much attention. Yet, higher U_C ($U_{C,H}$) may lead to a thinner concentration layer near CEM, sweeping out of concentrated stream near the membrane (Fig. 1c) and resulting in the reduction of surface concentration of cathodic side of CEM ($C_{S,C}$) and thinner δ_C , which will reduce any co-ion leakage from the concentrate side. This provides the experimental evidence regarding the mechanism behind CU lowering at high current, and offers ideas to mitigate this limitation

in system engineering.

In this work, we regulate the distribution of hydrodynamic flow in diluate and concentrate stream (i.e., U_D and U_C) independently and evaluate the influence of U_D and U_C on the current distribution, energy efficiency (voltage drop), and CU using the ICP process with return-flow spacer. Combined with numerical simulation, we provide experimental evidence for the mechanism of CU lowering, for the first time to our best knowledge.

2. Material and method

2.1. Device fabrication

The benchtop-scale ICP desalination with return-flow spacer was

used for experiments, and its configuration, fabrication, and operation were described and demonstrated in previous works (Kim et al., 2016; Yoon et al., 2019). The ICP desalination device comprises two electrode compartments and ICP compartment stacked up with alternating CEMs and spacers (Figure S1). The electrode compartments for anode and cathode are fabricated in clear cast acrylic frame, with Ru-Ir coated Titanium plates as electrodes (Baoji Qixin Titanium Co., LTD., China), sealed by silicon rubber. The ICP compartment is made of three spacers and two pieces of cation exchange membrane (Neosepta CMX, Astom Co., Japan) and two pieces of end membrane (FTCM, FuMA-Tech GmbH, Germany) with $5 \times 15 \text{ cm}^2$ of the effective membrane area.

2.2. System operation and measurement

Sodium chloride (S5886, Sigma-Aldrich, Co., St. Louis, MO, USA) solution with a concentration of 35 g/L was prepared for representative salinity for seawater. Sodium sulfate (239,313, Sigma-Aldrich, Co.) solution with a concentration of 0.6 M was used in the electrode rinsing channels. Two pumps, peristaltic pump (Masterflex® L/S pump, Cole-Parmer Instrument Company, LLC., Vernon Hills, IL) and circulation pump (McMaster) were used to apply the sodium chloride solution with various flow rates for feed flow and sodium sulfate solution with 300 mL/min for rinse, respectively. The constant current is applied by the DC power supply (9205, B&K Precision Cor., Yorba Linda, CA, USA). The voltage drop between spacers was measured by the digital multimeter (5491B, B&K Precision Cor.). The salinity changes at the outlet of diluate and concentrate streams were monitored by flow-through conductivity probe (16–900 Flow-thru Conductivity Electrode, Microelectrode, Inc., Bedford, NH, USA). Then, the diluate and concentrate solution are collected after the salinity changes have stabilized. The electrode conductivity cell (013610MD, Thermo Fisher Scientific Inc., Cambridge, MA, USA) measures the salinity of collected solutions.

2.3. Physicochemical transport model

The time-varying behavior of the system is dictated by continuity, which is given in this case as:

$$\frac{\partial c_i}{\partial t} + \nabla \cdot \mathbf{J}_i = 0, \quad (1)$$

where \mathbf{J}_i , and c_i are the molar flux density and molar concentration of ion i respectively. Chemical flux from diffusion, migration, and convection is given by the Nernst–Planck equations for dilute solutions:

$$\mathbf{J}_i = -D_i \left(\nabla c_i + \frac{z_i F}{RT} c_i \nabla \phi \right) + c_i \mathbf{u}, \quad (2)$$

where \mathbf{u} , ϕ , D_i , and z_i are the molar-averaged solvent velocity, electric potential, diffusivity, and charge number of ion i respectively. The electric potential is coupled to the space charge density through the Poisson equation:

$$\nabla \cdot \mathbf{E} = -\nabla^2 \phi = \frac{\rho_{SC}}{\epsilon_0 \epsilon_r} = \frac{F}{\epsilon_0 \epsilon_r} \sum_i z_i c_i, \quad (3)$$

where \mathbf{E} is the electric field vector, ρ_{SC} is the space charge, ϵ_0 is the permittivity of free space, and ϵ_r is the relative permittivity. The electric current density is given as:

$$\mathbf{i} = F \sum_i z_i \mathbf{J}_i, \quad (4)$$

which assumes displacement currents have a negligible effect. Finally, Navier–Stokes governs solvent transport:

$$\frac{\partial \mathbf{u}}{\partial t} + (\mathbf{u} \cdot \nabla) \mathbf{u} = -\frac{1}{\rho_w} \nabla p + \nu \nabla^2 \mathbf{u}, \quad (5)$$

where ρ_w is the solvent density, ν is the kinematic viscosity, and p is the pressure.

The main difference between the aqueous phase and the membrane itself, is that this region contains fixed negative charge of molar concentration, X . In other words,

$$\rho_{SC} = F \left(\sum_i z_i c_i - X \right), \quad (6)$$

throughout the membrane region. In order to speed up convergence, we given the membrane region initial conditions from solutions to an equilibrium model. In order to model galvanostatic polarization across the widths of the channels, we implement an electric field boundary condition at the boundary extending along $y = -W_M/2 - W_{CH}$ (Flavin et al., 2019).

All scaling, meshing, linear solving, and numerical integration was performed using the finite element method within COMSOL Multiphysics. See Section 3, supplementary information for further details relating to boundary conditions, assumptions, parameters, and numerical methods.

3. Result and discussion

3.1. Osmosis, back-diffusion, and water splitting cannot explain Cu lowering observed

Fig. 2a shows the general schematic of experimental system to evaluate the ICP process with various flow and current flux conditions. The flow rate for outlet of diluate (Q_D) and concentrate (Q_C) streams are controlled to have a target flow velocity by adjusting the flow control needle valves attached to the outlets. The effective voltage drop (V_{eff}) and the salinity of both diluate (C_D) and concentrate (C_C) streams are measured under an application of a given current flux. In the ICP architecture, we have the flexibility to control the flow speeds of both channels (U_D and U_C) independently, which was used to experimentally investigate the relationship between CU and the boundary layer thickness on both sides of the membrane. In Fig. 2b, experimentally removed salt flux ($J_{S,Exp}$) was compared with theoretically estimated chemical flux expected from various secondary mechanisms suggested previously (Andersen et al., 2012; Chehayeb et al., 2017; Frilette, 1957). The salt flux in ICP process ($J_{S,ICP}$) is derived the salt fluxes in ED ($J_{S,ED}$) described by a combination of electro-migration ($J_{S,ED} = A_M \frac{t_{S,ED}}{F} i$) and trans-membrane diffusion ($J_{S,M,D} = -A_M L_S \Delta C$) as follow:

$$J_{S,ED} = A_M \left(\frac{t_{S,ED}}{F} i - L_S \Delta C \right), \quad (7)$$

where A_M is the effective membrane area. $t_{S,ED}$ is the transference number of solute in ion-exchange membranes. F is the faraday's constant. i is the current flux. $L_S (= 1.083 \times 10^{-7} \text{ m/s})$ is the membrane constant for salt flux by diffusion (Fidaleo and Moresi, 2005). $t_{S,ED}$ is given by

$$\frac{t_{CEM}^+ + t_{AEM}^-}{2} \approx 1, \quad (8)$$

with an ideal permselectivity of ion exchange membranes. $t_{CEM}^+ \approx 1$ is the ideal transference number of cation in CEM and $t_{AEM}^- \approx 1$ is the ideal transference number of cation in AEM. The theoretical transference number for ICP process, employing only CEM ($t_{ICP, CEM}$), can be calculated as a control volume analysis (Figure S4, The detailed control volume analysis is described in Section 1, supplementary information). In the ICP process, outflux of solute comprise of electro- and diffusive migrations ($J_{S,m,ICP}$) as follow:

$$J_{S,m,ICP} = (t_{CEM}^+ - t^+ + t^-) \frac{I^c}{F}, \quad (9)$$

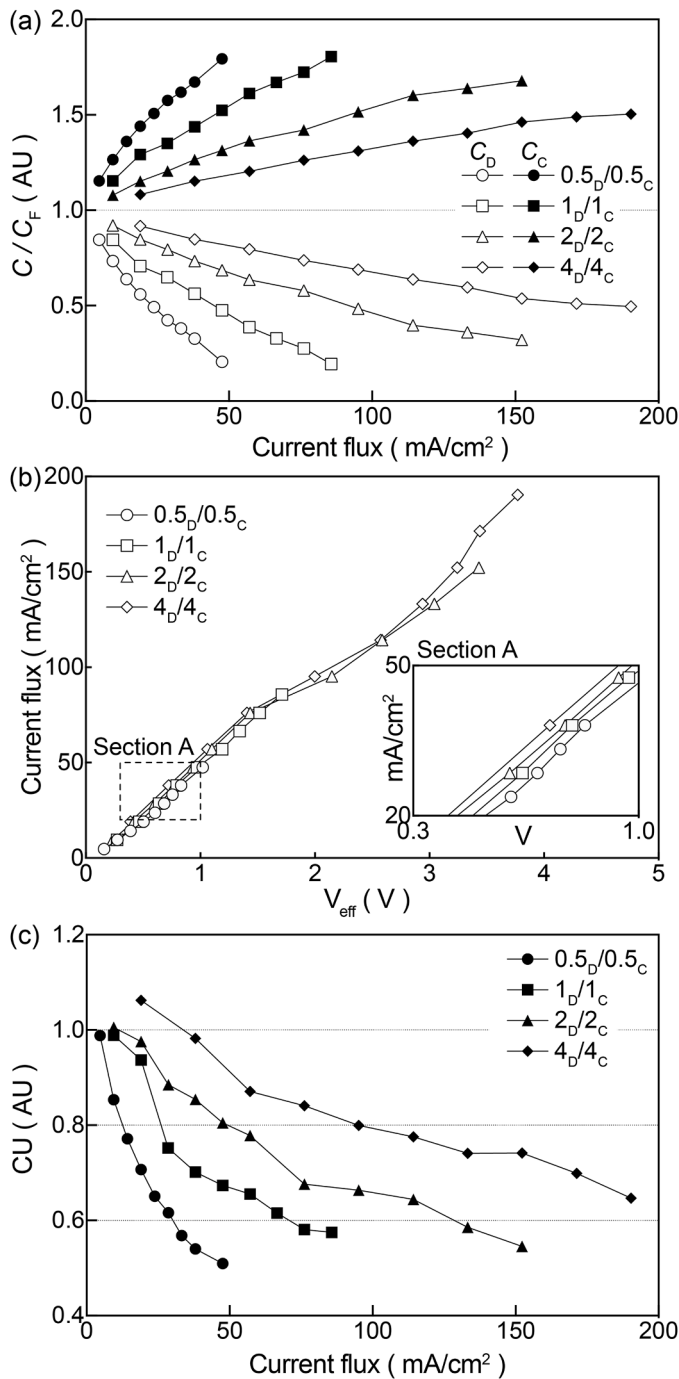


Fig. 3. (a) The salinity variation at the end of two streams, diluate (C_D) and concentrate (C_C) streams, (b) the I-V response and (c) the change in current utilization (CU) under various hydrodynamic convections as a function of current flux. A_D/B_C indicates the experiment condition with A mm/s of U_D and B mm/s of U_C .

where I^e is the net system current. t^+ and t^- are transference numbers of cation and anion, respectively. The sum of transference numbers is the overall transference number in the ICP process.

$$t_{ICP,CEM} = t_{CEM}^+ - t^+ + t^-, \quad (10)$$

where t_{CEM}^+ and $-t^+ + t^-$ represent the outflux by electro-migration and diffusive migration, respectively. The transference number of ICP process with sodium chloride can be written as following:

$$t_{ICP,CEM} = t_{CEM}^+ - t^{Na^+} + t^{Cl^-}, \quad (11)$$

where t^{Na^+} ($=0.393$) and t^{Cl^-} ($=0.606$) are transference number of sodium and chloride, respectively. Eq. (11) gives the result of the calculation of 1.213. In $t_{ICP,CEM}$, 0.213 is the advantage obtained by the diffusivity difference. The salt transport equation for the ICP process can be rewritten by following equation:

$$J_{S,ICP} = A_M \left(\frac{t_{ICP,CEM}}{F} i - L_S \Delta C \right), \quad (12)$$

If the ion exchange membranes remain an ideal permselectivity, one would expect that salt flux by migrations ($J_{S,m,ICP} = A_M \frac{t_{ICP,CEM}}{F} i$) would be the same as $J_{S,Exp}$. In reality, $J_{S,Exp}$ is always lower than $J_{S,m,ICP}$, yet one can see that the difference between them is increasing in proportion to the operating current. At the same diluate flow speed, CU is critically dependent on the flow speed of the concentrate flow speed. If the concentrate flow speed is set higher than that of diluate flow speed (2 mm/s of U_D with 4 mm/s of U_C , $2_D/4_C$, and $2_D/8_C$ conditions) one recovers near ideal CU values over a wide range of current density values (up to ~ 100 mA/cm²), effectively mitigating the issue of membrane selectivity loss. Interestingly, higher U_C (i.e., $2_D/8_C$) still allow to maintain high CU values even with a current flux beyond the limiting condition (areas shaded in gray in Fig. 2), compared to $2_D/4_C$ condition. In contrast, estimated secondary flux value such as back-diffusion ($J_{S,M,D}$), osmosis ($J_{W,M,O}$) and electro-osmosis ($J_{W,M,E}$) are found to be at least an order of magnitude smaller, casting doubts on the importance of these secondary transport processes. For example, $J_{S,M,D}$ (salt back-diffusion) is accounting for only 0.7% of $J_{S,M,E}$ in the case of $2_D/4_C$, even at the limiting current ($i_{L,2_D/4_C}$).

3.2. The effect of hydrodynamic convection in performance of ICP process

As previously reported (Yoon et al., 2019), the ICP process with the return-flow spacer shows a symmetrical variation of concentration profiles at C_D and C_C (Fig. 3a). To evaluate the system characteristic, we measure the current-voltage (I-V) response (Fig. 3b) and calculate the current utilization (CU, Fig. 3c), shown in the equation below:

$$CU = \frac{zFQ_D(C_F - C_D)}{I}, \quad (13)$$

where z is ion valence, F is Faraday's constant, and I is total current. As generally observed in the electro-membrane processes (i.e., ED and ICP), higher hydrodynamic flow velocity reduces resistance, promoting mass transfer through the formation of thin diffusion layers (Fig. 3c). Also, CU generally increases with higher hydrodynamic flow velocity, while decreases with an increase in the operating current (Fig. 3d). However, it is not clear which factor, ΔC or C_C , influences CU changes, since the symmetrical distribution of hydrodynamic convection ($Q_D = Q_C$) provides only a balanced change in C_D and C_C .

Therefore, we set out to assess the effect of hydrodynamic flow velocity in the concentrate stream (U_C) by testing various U_C values of 0.5 to 8 mm/s, with a fixed value of U_D at 2 mm/s (Fig. 4). The I-V response shows that higher U_C leads to increased cell resistance (Fig. 4a). However, higher U_C (at the same U_D and current values) leads to a dramatic reduction in the salinity of diluate output (C_D) (Fig. 4b), representing a significant improvement in CU (Fig. 4c and Figure S5). This result simply shows that the reduction in C_C allows improving CU as discussed in the previous paragraph. From Fig. 4d, one can see that lower C_C (caused by higher U_C values) is the main driving factor for maintaining high CU values, rather than ΔC or any boundary layer development in the diluate channel such as higher C_D .

3.3. Numerical analysis

In order to explore the phenomena discussed in this article more

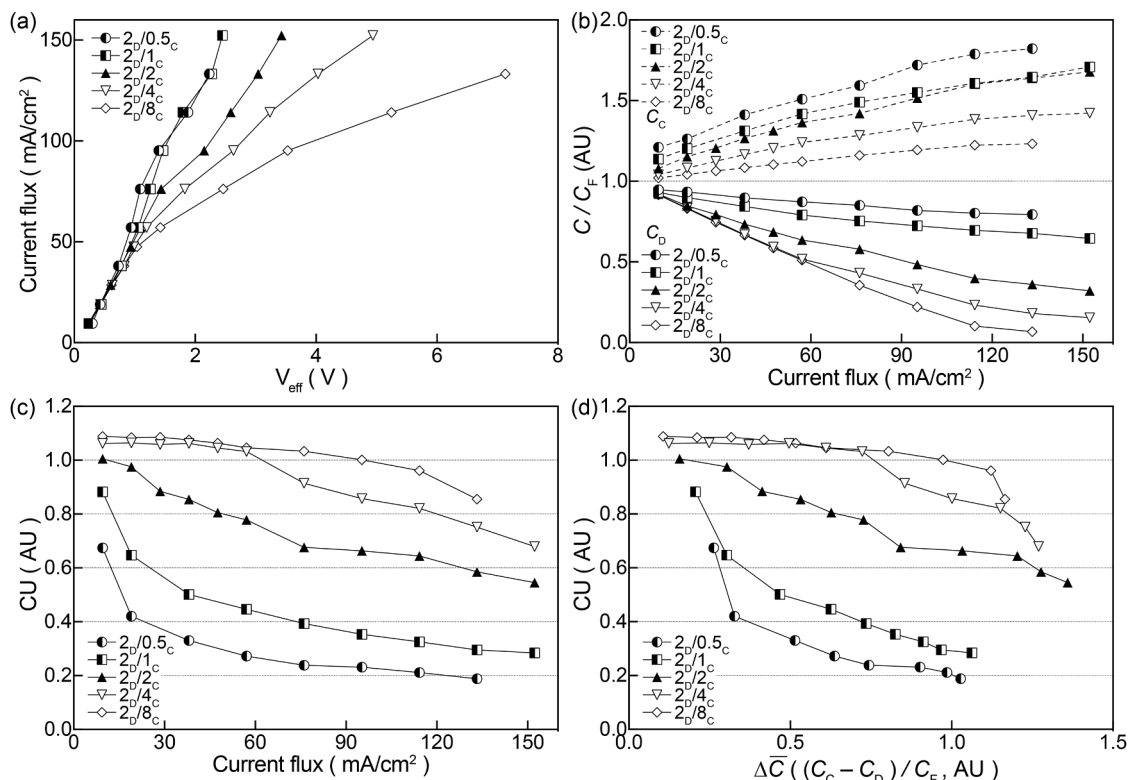


Fig. 4. (a) The I-V response and (b) the salinity variation of outlet of diluate (C_D) and concentrate (C_C) streams as a function of U_C with a fixed U_D as 2 mm/s versus the current flux. (c) The change in CU versus the current flux and (d) the concentration difference in C_C and C_D.

thoroughly, we supplemented our experiments with numerical simulations. These simulations focus specifically on processes in the concentrate stream that affect membrane transport—its selectivity in particular. We modeled ion and solvent transport throughout the three-region system using Nernst–Planck–Poisson and Navier–Stokes. The membrane itself was modeled as a region of fixed charge ($X = 5.7M$) with no permeability for solvent transport. For the applied current and flow conditions considered in the physical system, the membrane generates near-complete depletion in the diluted stream channel. Since the diluate stream and its respective phenomena are not the focus of our analysis here, we chose a sufficiently large diluted stream velocity, $U_D = 80$ mm/s, which renders boundary layer in the diluate channel almost negligible and numerically simplified the simulation significantly.

As demonstrated in Fig. 5a, the perpendicularly applied electric field ($\nabla\phi$) and solvent flow (U) generate a diffusion boundary layer on the concentrate side of the membrane, whose thickness increases along the length of the membrane. By the Gibbs–Donnan effect (Galama et al. 2013), this produces a larger concentration of both co- (C_{co-ion} , i.e., Cl^-) and counter-ions ($C_{counterion}$, i.e., Na^+) inside the membrane (Fig. 5b-i & ii) to maintain membrane electroneutrality ($C_{mem.} + C_{co-ion} = C_{counterion}$, $C_{mem.}$ is the charge density of membrane) (Geise et al., 2012). However, as shown in Fig. 5b-i, the co-ion concentration increases more substantially relative to its equilibrium value. This leads to the behavior shown in Fig. 5c-i and ii as the diffusion boundary layer thickness increases over the length of the membrane, the simulated permselectivity for counter-ion reduces substantially, allowing co-ion leakage. It is observed that the migration of co-ion (J_{M,Cl^-}) contributes to the majority of the co-ion flux (J_{Cl^-}), compared with the diffusion flux of co-ion (J_{D,Cl^-}) (Figure S7). Thus, as a whole, the membrane becomes less selective for counter-ion when a large ion enrichment layer is allowed to develop. As we can see in Fig. 5c-i, when we diminish this diffusion boundary layer by increasing the flow rate of the concentrate stream, the selectivity (as described by integral transference, $T_i = J_i / \sum_k J_k$) converges to the ideal

case—unity transference for counter-ion and 1.2 of current utilization for ICP process (Fig. 5d). Ultimately, this explains why we experience better membrane performance under higher U_C.

4. Conclusion

Herein, we demonstrate the influence of hydrodynamic convective flow on the ion transport in the electromembrane process. The increase in hydrodynamic flow in concentrate stream leads to a reduction in the ion concentration near the membrane. Subsequently, it results in improved electromembrane process (i.e., higher current utilization and more uniform current distribution). This mechanism is clearly validated by both experiments and numerical simulation. In addition, the benefit of higher U_C is maximized in the operating condition beyond the limiting current regime where a thicker concentration layer is inevitably developed. The numerical simulation shows that a lower U_C leads to a thicker diffusion layer on the cathodic side of cation exchange membrane, while increasing both co- and counter-ions in the membrane to maintain its electroneutrality. This increase in co-ion concentration increases the leakage migration of co-ions, diminishing the transference of membrane. While the concept presented here was demonstrated using ICP desalination process only, it is clear that other desalination processes such as ED can also benefit from the same strategy to achieve higher CU and energy efficiency, perhaps at the cost of lower recovery rate (from the fast flow in the concentrate channel). At the same time, in our simulation result, we note that counter-ion transport is largely unaffected even under the fast concentrate stream flow, which may be an optimal operating condition with better energy efficiency for certain desalination applications (e.g., portable scale desalination).

Declaration of Competing Interest

The authors declare that they have no known competing financial interests or personal relationships that could have appeared to influence

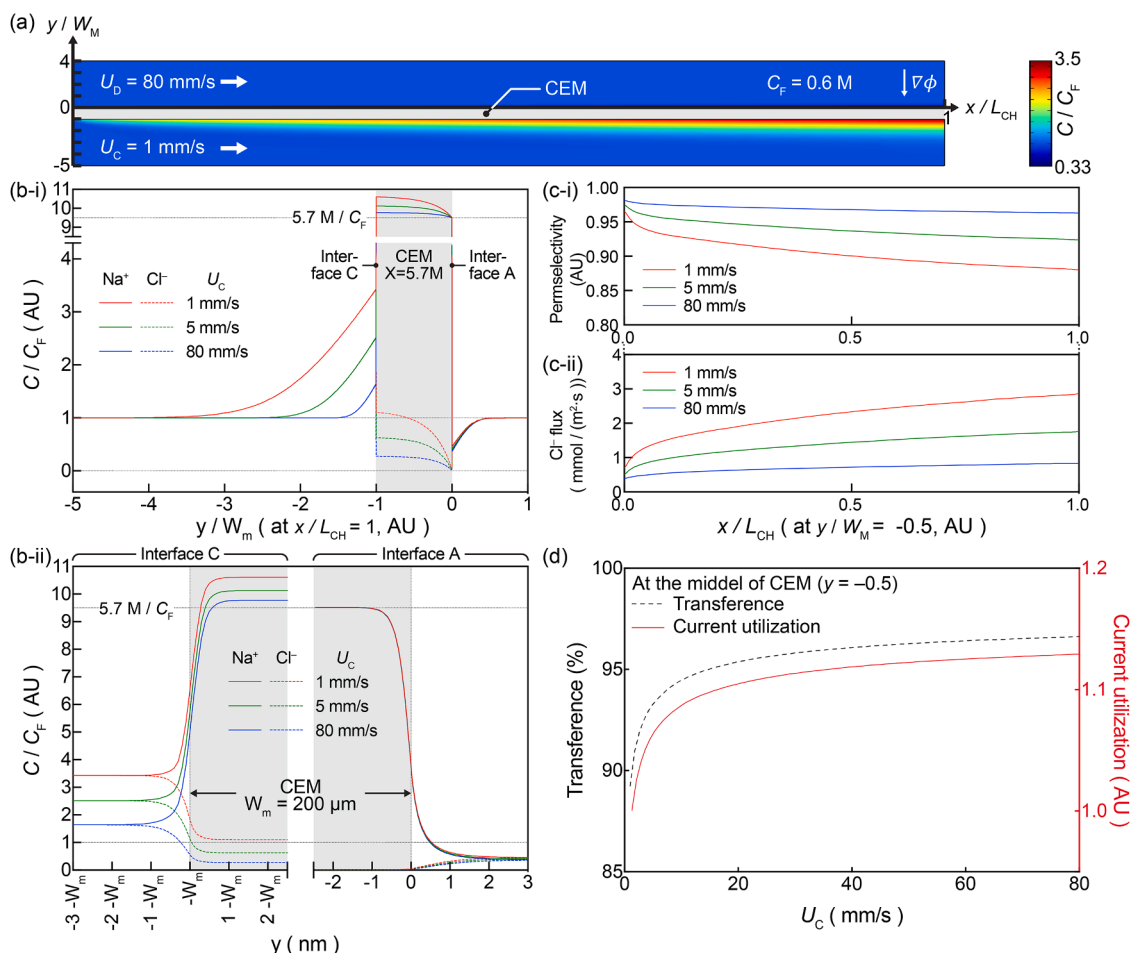


Fig. 5. The result of numerical analysis. (a) The visualized magnitude of concentration profile of the diluate and concentrate streams (The concentration of CEM is excluded for visualization purpose). (b-i) The change in concentration profile across the membrane as a function of U_c and (b-ii) the concentration profile at interface of anodic (Interface A) and cathodic side (Interface C) of CEM. The change in (c-i) the permselectivity and (c-ii) the co-ion flux along CEM (See Figure S7 in ESI, for the migration and the diffusion fluxes of chloride). (d) The changes in the integral transport characteristics of the membrane and the current utilization as a function of U_c .

the work reported in this paper.

Acknowledgements

The authors acknowledge the contributions of Eric Brack from U.S. Army Combat Capabilities Development Command (DEVCOM) - Soldier Center for valuable suggestions and constructive comments as a technical advisor. This work was partially supported by Kuwait Foundation for the Advancement of Sciences (KFAS) for their financial support through Project No. P31475EC. Also, it is supported by DEVCOM - Soldier Center (Individual Water Desalination and Purification project, Project No.17.316) with the Public Release Approval number (PAO #: U21–213). Matthew Flavin was supported by the Draper Fellowship.

Supplementary materials

Supplementary material associated with this article can be found, in the online version, at [doi:10.1016/j.watres.2021.117351](https://doi.org/10.1016/j.watres.2021.117351).

References

abu-Rjal, R., Chinarian, V., Bazant, M.Z., Rubinstein, I., Zaltzman, B., 2014. Effect of concentration polarization on permselectivity. *Phys. Rev. E* 89, 12302. <https://doi.org/10.1103/physreve.89.12302>. PMID - 24580222.

Al-anzi, B., Al-hammadi, S., Yoon, J., Han, J., 2020. Techno-economic analysis of multi-stage ion concentration polarization with recirculation for treatment of oil produced

water. *J. Environ. Manage.* 269, 110788. <https://doi.org/10.1016/j.jenvman.2020.110788>.

Andersen, M.B., van Soestbergen, M., Mani, A., Bruus, H., Biesheuvel, P.M., Bazant, M.Z., 2012. Current-induced membrane discharge. *Phys. Rev. Lett.* 109, 108301. <https://doi.org/10.1103/PhysRevLett.109.108301>.

Balster, J., Pünt, I., Stamatialis, D.F., Wessling, M., 2006. Multi-layer spacer geometries with improved mass transport. *J. Memb. Sci.* 282, 351–361. <https://doi.org/10.1016/j.memsci.2006.05.039>.

Balster, J., Stamatialis, D., Wessling, M., 2010. Membrane with integrated spacer. *J. Memb. Sci.* 360, 185–189. <https://doi.org/10.1016/j.memsci.2010.05.011>.

Chehayeb, K.M., Farhat, D.M., Nayar, K.G., Lienhard, J.H., 2017. Optimal design and operation of electrodesalination for brackish-water desalination and for high-salinity brine concentration. *Desalination* 420, 167–182. <https://doi.org/10.1016/j.desal.2017.07.003>.

J.H. Choi, S., Kim, B., Nayar, K.G., Yoon, J., Al-Hammadi, S., Lienhard, V., Han, J., Al-Anzi, B., Al-hammadi, S., V, J.H.L, Han, J., Al-Anzi, B., 2019. Techno-economic analysis of ion concentration polarization desalination for high salinity desalination applications *Water Res* 155, 162–174. <https://doi.org/10.1016/j.watres.2019.02.023>. PMID - 30849730.

Doornbusch, G., Swart, H., Tedesco, M., Post, J., Borneman, Z., Nijmeijer, K., 2020. Current utilization in electrodesalination: electrode segmentation as alternative for multistaging. In: *Desalination*, 480, 114243. <https://doi.org/10.1016/j.desal.2019.114243>.

Doornbusch, G.J., Tedesco, M., Post, J.W., Borneman, Z., Nijmeijer, K., 2019. Experimental investigation of multistage electrodesalination for seawater desalination. *Desalination* 464, 105–114. <https://doi.org/10.1016/j.desal.2019.04.025>.

Fidaleo, M., Moresi, M., 2006. Electrodesalination Applications in the food industry. *Adv. Food Nutr. Res.* 51, 265–360. [https://doi.org/10.1016/s1043-4526\(06\)51005-8](https://doi.org/10.1016/s1043-4526(06)51005-8). PMID - 17011478.

Fidaleo, M., Moresi, M., 2005. Optimal strategy to model the electrodesalination recovery of a strong electrolyte. *J. Memb. Sci.* 260, 90–111. <https://doi.org/10.1016/j.memsci.2005.01.048>.

- Flavin, M.T., Freeman, D.K., Han, J., 2019. Interfacial ion transfer and current limiting in neutral-carrier ion-selective membranes: a detailed numerical model. *J. Memb. Sci.* 572, 374–381. <https://doi.org/10.1016/j.memsci.2018.10.065>.
- Frilette, V.J., 1957. Electrogravitational transport at synthetic ion exchange membrane surfaces. *J. Phys. Chem.* 61, 168–174. <https://doi.org/10.1021/j150548a010>.
- Geise, G.M., Falcon, L.P., Freeman, B.D., Paul, D.R., 2012. Sodium chloride sorption in sulfonated polymers for membrane applications. *J. Memb. Sci.* 424, 195–208. <https://doi.org/10.1016/j.memsci.2012.08.014>, 423–.
- Jiang, C., Wang, Y., Zhang, Z., Xu, T., 2014. Electrodialysis of concentrated brine from RO plant to produce coarse salt and freshwater. *J. Memb. Sci.* 450, 323–330. <https://doi.org/10.1016/j.memsci.2013.09.020>.
- Kim, B., Kwak, R., Kwon, H.J., Pham, V.S., Kim, M., Al-Anzi, B., Lim, G., Han, J., 2016. Purification of high salinity brine by multi-stage ion concentration polarization desalination. *Sci. Rep.* 6, 31850. <https://doi.org/10.1038/srep31850>. PMID - 27545955.
- Kim, B., Kwon, H., Ko, S.H., Lim, G., Han, J., 2017. Partial desalination of hypersaline brine by lab-scale ion concentration polarization device. *Desalination* 412, 20–31. <https://doi.org/10.1016/j.desal.2017.02.018>.
- Korngold, E., Aronov, L., Daltrophe, N., 2009. Electrodialysis of brine solutions discharged from an RO plant. *Desalination* 242, 215–227. <https://doi.org/10.1016/j.desal.2008.04.008>.
- Kwak, R., Guan, G., Peng, W.K., Han, J., 2013. Microscale electrodialysis: concentration profiling and vortex visualization. *Desalination* 308, 138–146. <https://doi.org/10.1016/j.desal.2012.07.017>.
- Kwak, R., Pham, V.S., Kim, B., Chen, L., Han, J., 2016. Enhanced salt removal by unipolar ion conduction in ion concentration polarization desalination. *Sci. Rep.* 6, 25349. <https://doi.org/10.1038/srep25349>. PMID - 27158057.
- La Cerva, M., Gurreri, L., Tedesco, M., Cipollina, A., Ciofalo, M., Tamburini, A., Micale, G., Cerva, M., La Gurreri, L., Tedesco, M., Cipollina, A., Ciofalo, M., Tamburini, A., Micale, G., 2018. Determination of limiting current density and current efficiency in electrodialysis units. *Desalination* 445, 138–148. <https://doi.org/10.1016/j.desal.2018.07.028>.
- Moya, A.A., 2016. A numerical comparison of optimal load and internal resistances in ion-exchange membrane systems under reverse electrodialysis conditions. *Desalination* 392, 25–33. <https://doi.org/10.1016/j.desal.2016.04.016>.
- Nakayama, A., Sano, Y., Bai, X., Tado, K., 2017. A boundary layer analysis for determination of the limiting current density in an electrodialysis desalination. *Desalination* 404, 41–49. <https://doi.org/10.1016/j.desal.2016.10.013>.
- Nikonenko, V.V., Pismenskaya, N.D., Belova, E.I., Sistas, P., Huguet, P., Pourcelly, G., Larchet, C., 2010. Intensive current transfer in membrane systems: modelling, mechanisms and application in electrodialysis. *Adv. Colloid Interface Sci.* 160, 101–123. <https://doi.org/10.1016/j.cis.2010.08.001>.
- Rubinstein, I., Shtilman, L., 1979. Voltage against current curves of cation exchange membranes. *J. Chem. Soc. Faraday Trans. 2 Mol. Chem. Phys.* 75, 231. <https://doi.org/10.1039/f29797500231>.
- Sadrzadeh, M., Mohammadi, T., 2008. Sea water desalination using electrodialysis. *Desalination* 221, 440–447. <https://doi.org/10.1016/j.desal.2007.01.103>.
- Shaposhnik, V.A., Kuzminykh, V.A., Grigorichuk, O.V., Vasil'eva, V.I., 1997. Analytical model of laminar flow electrodialysis with ion-exchange membranes. *J. Memb. Sci.* 133, 27–37. [https://doi.org/10.1016/S0376-7388\(97\)00063-x](https://doi.org/10.1016/S0376-7388(97)00063-x).
- Shaposhnik, V.A., Vasil'eva, V.I., Praslov, D.B., 1995. Concentration fields of solutions under electrodialysis with ion-exchange membranes. *J. Memb. Sci.* 101, 23–30. [https://doi.org/10.1016/0376-7388\(94\)00270-9](https://doi.org/10.1016/0376-7388(94)00270-9).
- Strathmann, H., 2010. Electrodialysis, a mature technology with a multitude of new applications. *Desalination* 264, 268–288. <https://doi.org/10.1016/j.desal.2010.04.069>.
- Tadimeti, J.G.D., Kurian, V., Chandra, A., Chattopadhyay, S., 2016. Corrugated membrane surfaces for effective ion transport in electrodialysis. *J. Memb. Sci.* 499, 418–428. <https://doi.org/10.1016/j.memsci.2015.11.001>.
- Tanaka, Y., 2000. Current density distribution and limiting current density in ion-exchange membrane electrodialysis. *J. Memb. Sci.* 173, 179–190. [https://doi.org/10.1016/S0376-7388\(00\)00368-9](https://doi.org/10.1016/S0376-7388(00)00368-9).
- Tedesco, M., Hamelers, H.V.M., Biesheuvel, P.M., 2016. Nernst-Planck transport theory for (reverse) electrodialysis: I. Effect of co-ion transport through the membranes. *J. Memb. Sci.* 510, 370–381. <https://doi.org/10.1016/j.memsci.2016.03.012>.
- Yan, H., Wang, Y., Wu, L., Shehzad, M.A., Jiang, C., Fu, R., Liu, Z., Xu, T., 2019. Multistage-batch electrodialysis to concentrate high-salinity solutions: process optimisation, water transport, and energy consumption. *J. Memb. Sci.* 571, 245–257. <https://doi.org/10.1016/j.memsci.2018.10.008>, 570–.
- Yoon, J., Do, V.Q., Pham, V.-S., Han, J., 2019. Return flow ion concentration polarization desalination: a new way to enhance electromembrane desalination. *Water Res* 159, 501–510. <https://doi.org/10.1016/j.watres.2019.05.042>. PMID - 31129480.